A Theoretical Description of Integrated OAM Beam Emitters Using Conical Wave Model

Zihao Zhi, Yingzhi Li, Baisong Chen, Xiaobin Liu, Xuetong Li, Lanxuan Zhang [ID], Yuxuan Li, Quanxin Na,
Qijie Xie [ID], Xueyan Li [ID], Fengli Gao [ID], and Junfeng Song [ID]

Abstract—A theoretical model, suitable for multiple structures of integrated vortex beam emitters, is proposed, developed and verified. Using the interference superposition of multiple plane waves in the far-field plane, which have the same wavevector in the z-direction, the expressions of the orbital angular momentum (OAM) beam field emitted from integrated devices are obtained. The results are applicable to OAM beams with larger or fractional topological charges, and consider different initial polarization states, which means different structures. Especially, when $\vartheta = 0, p = 0$, the result is the same as those derived from the dipole model and is consistent with the previous experimental results. The calculated results show that it can obtain more accurate far-field light field with topological charge l increasing gradually and gain the same Ex and Ey with different initial polarization states. By constructing this model, the generation mechanism of the integrated OAM beam emitters can be easily understood and the beam vortex can be generated naturally and flexibly.

Index Terms—Orbital angular momentum (OAM), photonic integrated circuits, optical beams, integrated optics, vortex beam.

I. INTRODUCTION

INTEGRATED OAM vortex beam emitter [1]–[9], with its advantages of small footprint, tunability and large-scale mass production, has become an important method for vortex beam generation. Lots of Integrated emitters, like microring resonator [1]–[4] or cobweb structure [5]–[9] have been made, which usually use emission points to send out wavelets. They interfere

in space to procedure OAM vortex beam. However, there are few theoretical studies on OAM beam generated by those devices because it is difficult to describe the process by using distinct and straightforward formulas. So far, some theoretical models on integrated OAM vortex beam emitter have been studied like, coupled mode theory (CMT) [1], [10], [11], which can explicitly explain the physical mechanism of mode coupling, but it needs to solve complex coupled-mode equations and spend lots of energy to find the coupling coefficient in many modes. Three-dimensional Finite Difference Time Domain numerical method (3D-FDTD) [8], [12]–[14] is also came up, which can catch simulation results by high-performance computer, but it is difficult to distinguish the physical mechanism. Dipole model [15], [16] is used to replace the beam-emitting sources directly with dipole oscillators. Although, it can well verify the experimental results when topological charge l is small, the equation introduces some quantities independent on light as dipole moment such that, it is very limited in larger or fractional l due to the approximations are made in the solution process, like integral approximation, Fresnel diffraction approximation etc. Moreover, CMT and Dipole model are only applicable to microring resonator structure which means integer topological charges. 3D-FDTD is only used to calculate small size effectively and the devices with a radius of more than 30 um can hardly be analyzed (part 3 in [14]). Therefore, an accurate, intuitive and comprehensive theory needs to be proposed, by which to calculate the larger or fractional l precisely and large-scale structures faster. The theory also takes different initial polarization of the emission into consideration.

In this Letter, a multi-plane wave interference model [17] suitable for various structures is proposed, proved and verified for the integrated OAM beam emitters. It replaces each emission grating with a plane wave source instead of dipole oscillator and start directly from the light field of plane wave instead of dipole moment. In fact, it has been proved experimentally that the light emitted from the grating can approximate to a plane wave in the far field [17, Fig. 6(a)]. Due to the same polarization along the z-axis of the beam emitted by each sub wave source, the magnitude of radial polarization is the same, and the direction is related to the position of emission point, that is conical wave (the name from [18] or conical wavefronts in [19]) we call it conical wave model (CWM). Through rigorous calculation, the expressions of the radiated light field are obtained. In particular, when $\vartheta = 0, p = 0$ the results are same as those derived from the dipole model and they are also demonstrated the beam from the
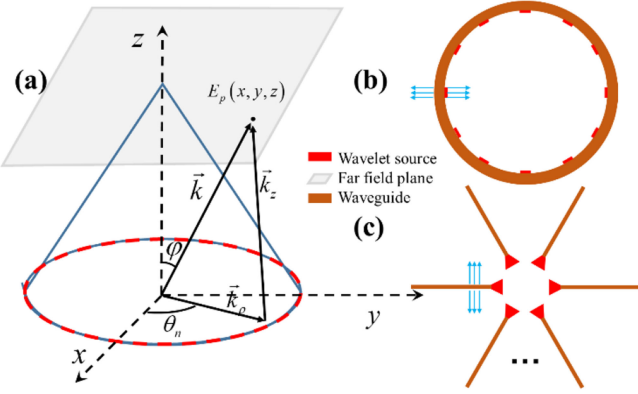
Fig. 1. (a) Schematic illustration of CWM for integrated emitters. (b) Schematic of microring resonator structure. (c) Cobweb structure.

integrated emitters is formed from left-handed circularly polarized (LHCP) light of charges $l - 1$ and right-handed circularly polarized (RHCP) light of charges $l + 1$. In order to showcase the advantages of the model, we use cosine similarity to compare the intensity and phase images obtained by different models qualitatively and quantitatively. The results show that when l increases gradually, the discrepancies between the models gradually enlarge, attributing to the failure in approximate conditions in the dipole model. In addition, we also use this model to analyze the fractional OAM beam, showing be consistent with the previous simulation and experimental results. Finally, the far-field interference results of wavelet with different primary polarization states are numerically calculated, it demonstrates that they have the same E_x and E_y, and when they interfere with the spherical wave, the difference of the initial polarization state will be shown.

II. METHODS

The schematic diagram of the CWM for integrated emitters is illustrated in Fig. 1(a). The emitted plane wave from multiple sub wave sources (red area) interfere in the far field (gray area) to form OAM beam. Fig. 1(b) and (c) show the microring resonator and cobweb structure [8], [20] similar shapes are called circular grating coupler in [21]–[23], which have different polarization state distribution (blue arrow line), since the beam in TE mode is perpendicular to the propagation direction of the waveguide (dark orange area). Thanks to the size of the grating element is very small compared to wavelength [1], [2], the spherical wave emitted by sub-wavelength grating can be approximated as plane wave under paraxial and far-field conditions. The electric field distribution of the plane wave emitted by the nth sub wave source is:

$$\vec{E}_{l,n} = a_n \exp\left(i\vec{k}_n\left(\vec{r} - \vec{r}_n\right) + il\theta_n\right), \quad (1)$$

Where a_n is the amplitude of nth plane wave, i is the imaginary number of units, $\vec{k}_n = k(\sin\varphi\cos(\theta_n + \vartheta)$, $\sin\varphi\sin(\theta_n + \vartheta), \cos\varphi)$ is the wavevector for nth field, $\vec{r} = x\vec{x} + y\vec{y} + z\vec{z}$ is the position vector, l is the topological charge of OAM vector beams, $\theta_n = 2\pi n/N$ is the azimuthal angles. What's more, $\varphi = \arcsin(k_\rho/k)$ is the polar angle and half of the apex angle of the cone in Fig. 1(a), $k = 2\pi/\lambda$ is the wavenumber and $k^2 = k_\rho^2 + k_z^2$, N is the total number of sub wave sources, λ is the wavelength of plane beam in vacuum, ϑ is an angle controlling the polarization direction, with a value from 0 to $\pi/2$, which corresponds to the microring resonator structure when $\vartheta = 0$ and for cobweb structure when $\vartheta = \pi/2$. Therefore, the OAM beam field in far field plane is:

$$\vec{E}_l = \begin{pmatrix} E_{l,x} \\ E_{l,y} \end{pmatrix} = \sum_{n=1}^{N} a_n \begin{pmatrix} \sin(\theta_n + \vartheta) \\ -\cos(\theta_n + \vartheta) \end{pmatrix} \exp$$

$$\left[i\vec{k}\cdot\left(\vec{r} - \vec{r}_n\right) + il\theta_n\right], \quad (2)$$

Since the coordinates of the light source point are $(x_n, y_n, 0) = R(\cos\theta_n, \sin\theta_n, 0)$, here R is the radius of the device and the coordinates of the far-field image point are $(x, y, z) = (\rho\cos u, \rho\sin u, z)$, using the mathematical expression $e^{ix\cos\theta} = \sum_{m=-\infty}^{m=\infty} J_m(x)i^m e^{im\theta}$, here $J_m(x)$ is the first kind of Bessel function. Eq. (2) can be cast into the following form:

$$\vec{E}_l = A \sum_{m=-\infty}^{+\infty} \left\{ J_m(k_\rho\rho)i^m \exp(-imu) \right.$$

$$\left. \times \sum_{n=1}^{N} \begin{pmatrix} \sin(\theta_n + \vartheta) \\ -\cos(\theta_n + \vartheta) \end{pmatrix} \exp\left[im(\theta_n + \vartheta) + il\theta_n\right] \right\}, \quad (3)$$

Where $A = a_n \exp(ik_z z)\exp[-ik_\rho R\cos(\vartheta)]$, and we define $\Delta\theta = 2\pi/N$, $B^\pm = (m + l \pm 1)\Delta\theta$, which will have no effect on the result except in appearance. By using the Euler's formula in complex function, we obtain Eq. (4).

$$\vec{E}_{l,x} = A \sum_{m=-\infty}^{+\infty} \left\{ \frac{1}{2i} J_m(k_\rho\rho)i^m \exp(im\vartheta - imu) \right.$$

$$\left. \begin{pmatrix} \frac{\exp(i\vartheta)\exp\left[\frac{1}{2}i(N-1)B^+\right]\sin\left(\frac{NB^+}{2}\right)}{\sin\left(\frac{B^+}{2}\right)} - \\ \frac{\exp(-i\vartheta)\exp\left[\frac{1}{2}i(N-1)B^-\right]\sin\left(\frac{NB^-}{2}\right)}{\sin\left(\frac{B^-}{2}\right)} \end{pmatrix} \right\}, \quad (4)$$

When l is an integer, we have $\sin(NB^+/2) = \sin[\pi(m + 1 + l)] \equiv 0$, and we can catch $\sin(NB^+/2)/\sin(B^+/2) = N\delta(pN - l - 1 - m)$ Here p is an integer and $\delta(x)$ is the delta function (see (5) at the bottom of this page).

$$\vec{E}_{l,y} = \frac{A}{-2} \sum_{m=-\infty}^{+\infty} \left\{ J_m(k_\rho\rho)i^m \exp(im\vartheta - imu) \begin{bmatrix} \exp(i\vartheta)\exp\left[\frac{1}{2}i(N-1)B^+\right]N\delta(pN - l - 1 - m) + \\ \exp(-i\vartheta)\exp\left[\frac{1}{2}i(N-1)B^-\right]N\delta(pN - l + 1 - m) \end{bmatrix} \right\}, \quad (5)$$

Finally, we attach the far-field electric field Eq. (6),

$$\vec{E}_l = \begin{pmatrix} E_{l,x} \\ E_{l,y} \end{pmatrix}$$

$$= \frac{AN}{2i} \sum_{p=-\infty}^{+\infty} \left\{ (-1)^{(N-1)p} \exp\left[i\vartheta\left(pN - l\right)\right] i^{pN-l-1} \right.$$

$$\left\{ \{J_{pN-l-1}\left(k_\rho \rho\right) \exp\left[-iu\left(pN - l - 1\right)\right]\} \begin{pmatrix} 1 \\ -i \end{pmatrix} \right.$$
$$\left. \left. + \{J_{pN-l+1}\left(k_\rho \rho\right) \exp\left[-iu\left(pN - l + 1\right)\right]\} \begin{pmatrix} 1 \\ i \end{pmatrix} \right\} \right\}, \tag{6}$$

Equation (6) indicates that the OAM beam from integrated emitter consists of $(l - pN) - 1$ order LHCP light and $(l - pN) + 1$ order RHCP light. For clarity, RHCP light is discussed by default when the following analysis is not explicitly described. Particularly, when $\vartheta = 0$, $p = 0$ and using the math formula $J_{-m}(x) = (-1)^m J_m(x)$, we obtain Eq. (7) from Eq. (6), which is same as the reported result (Eq. (9) in [15], Eq. (7) in [16]) and be consistent to the experimental results in Res [1].

$$\vec{E}_l = \frac{AN}{2} i^l \left\{ J_{l+1}\left(k_\rho \rho\right) \exp\left[iu\left(l + 1\right)\right] \begin{pmatrix} 1 \\ -i \end{pmatrix} \right.$$
$$\left. + J_{l-1}\left(k_\rho \rho\right) \exp\left[iu\left(l - 1\right)\right] \begin{pmatrix} 1 \\ i \end{pmatrix} \right\}, \tag{7}$$

For microring resonator structure with M_q gratings in Fig. 1(b) (M_q is an integer), when a stable mode is formed in the microring, there is the following relationship $2\pi R n_{eff} = M_p \lambda$, here M_p is an integer and n_{eff} is the effective refractive index of the device. The phase difference of light waves emitted by adjacent gratings is $\Delta\theta = 2\pi M_p/M_q$. Since the topological charge of this structure is $l = M_p - M_q$ [1]. Finally, We can get the phase of this structure in the CWM model.

$$l\theta_n = (M_p - M_q) 2\pi n M_p/M_q, \tag{8}$$

For cobweb structure in Fig. 1(c), since the phase of each emission source can be controlled separately, it does not need to meet the resonance condition, as long as the phase between adjacent emission beams is maintained at $\Delta\theta = 2\pi/N$, vortex beams can be emitted, and the order of topological charge is not necessarily integer.

III. RESULTS

In order to demonstrate the disparity between the Eq. (6) (CWM) and Eq. (7) (Dipole model) in detail, we use cosine similarity to calculate them more accurately, which has been used to study optical frequency comb [24] and optical phased array [25] for quantitatively. Consider two known vectors $\vec{a} = (x_1, x_2, \ldots, x_K), \vec{b} = (y_1, y_2, \ldots, y_K)$, and their cosine similarity can be expressed as Eq. (9) ranging from 0 to 1, which means weaker correlation and strong correlation or exactly same between two vectors. The similarity between two pictures by
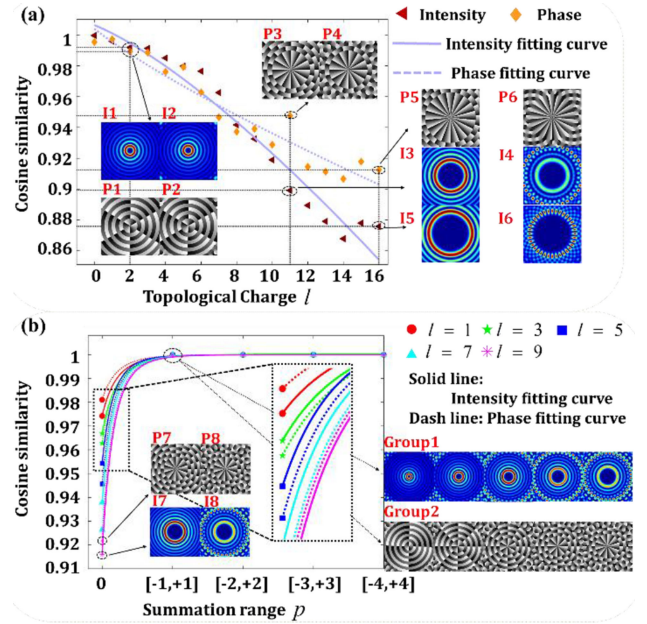

Fig. 2. Comparison of cosine similarity between two images when $\vartheta = 0$. (a) The cosine similarity of light intensity (dark red triangle), phase (orange diamond) changes with topological charges from 0 to 16 between $p = 0$ and $p = 0, \pm 1$ in Eq. (6), the solid and dash line are intensity and phase fitting curve, the insets (I1-I6, P1-P6) are intensity or phase diagrams of the corresponding points. (b) The cosine similarity of light intensity (solid line), phase (dash line) changes with the summation range p, pictures compared to them are the ideal (p ranges from -20 to 20) light intensity and phase pattern which have the same topological charge number, different colors correspond to different orders of topological charges as $l = 1, 3, 5, 7, 9$ respectively, the insets (I7, I8, P7, P8) are intensity or phase diagrams of the corresponding points, the Group1 and Group2 are the intensity and phase for $p = 0, \pm 1$ and $l = 1, 3, 5, 7, 9$ respectively.

different models can be quantitatively evaluated using the cosine similarity.

$$\cos(a, b) = \frac{\sum_{k=1}^{K} x_k y_k}{\sqrt{\sum_{k=1}^{K} x_k^2} \sqrt{\sum_{k=1}^{K} y_k^2}}. \tag{9}$$

To a specific device with $R = 3.9 \, um \, N = 36$ and the maximum OAM beam's order is 2 (see Fig. 2S(a) in [1]), there is no difference between the results by Eq. (6) [I2 and P2 in Fig. 2(a)] and Eq. (7) [I1 and P1 in Fig. 2(a)] due to the l is small relative to N. Their cosine similarity is 0.9919 for light intensity and 0.9893 for light phase. However as is shown in Fig. (2a) with l getting bigger and bigger, the dissimilarity will become more and more serious. The light intensity I5 (simulation by dipole model) and I6 (by conical wave model), P5 (by dipole model) and P6 (by conical wave model) in Fig. 2(a) are markedly different, the cosine similarity is 0.8758 for light intensity and 0.9126 for light phase, which is one of the advantages of our model over the dipole model. What's more, the dipole model may break down at some points, for example the intensity and phase with $l = 35$ (even $l = 20$), $N = 36$ can be obtained by Eq. (7), however, the result is contrary to reality. The strange result arises from approximations in dipole model, and obviously, the approximate conditions are void this case. There is an abnormal point [P3 and P4 in Fig. 2(a)] in the above phase calculation, which may come from the size interception of the calculated picture or the setting

of simulation parameters, but it does not affect the conclusion that the cosine similarity gradually decreases with the increase of topological charge, which means that using the dipole model to calculate larger l will produce larger error in theory. This deviation from the dipole model theory will affect the light field scattering force [26], the gradient force [27] in optical micromanipulation [28] and the purity of OAM mode [16] in high-capacity optical communication [29] or high-security encryption [30], that is, the error rate of communication will increase greatly. There is no doubt that the use of dipole model will bring some strange problems to specific devices, especially when l is larger, which will limit the application of OAM beam.

Although p takes an integer from negative infinity to positive infinity in Eq. (6), it is sufficient when $p = 0, \pm 1$ since the value of higher-order Bessel function is very small. We quantitatively analyzed the light intensity, phase using Eq. (6) when $p = 0$; $p = 0, \pm 1$; $p = 0, \pm 1, \pm 2$; $p = 0, \pm 1, \pm 2, \pm 3$; $p = 0, \pm 1, \pm 2, \pm 3, \pm 4$ respectively, and compared it with the ideal light intensity and phase diagram (p ranges from -20 to 20). As shown in Fig. 2(b) when $p = 0$, with the increase of topological charge l, the value of cosine similarity becomes smaller and smaller whether for light intensity or phase, the values are 0.9742, 0.9668, 0.9543, 0.9378, 0.9160 for intensity and 0.9810, 0.9627, 0.9456, 0.9264, 0.9217 for phase with $l = 1, 3, 5, 7, 9$. Especially I7 (calculated with $p = 0$), I8 (p from -20 to 20) are the calculated picture for the light intensity of $l = 9$ in Fig. 2(b), and P7 ($p = 0$), P8 (p from -20 to 20) are for the light phase of $l = 9$. However, when $p = 0, \pm 1$ the values of their cosine similarity are all 1 after retaining 12 decimal places, which means that the results are the same as those from p ranges from -20 to 20, here the calculated pictures are marked in Group1 (for light intensity) and Group2 (for light phase) with $l = 1, 3, 5, 7, 9$ respectively. In addition, we also calculated $p = 0, \pm 1, \pm 2$; $p = 0, \pm 1, \pm 2, \pm 3$; $p = 0, \pm 1, \pm 2, \pm 3, \pm 4$ in order to avoid accidental errors in Fig. 2(b), which are the same as the result of $p = 0, \pm 1$. Finally, we still keep p from $-\infty$ to $+\infty$ in Eq. (6) for generality in engineering and rigorous on mathematical.

Emitters based on the microring resonator structure cannot release OAM beams with fractional topological charges since $l = M_p - M_q$ is an integer. The dipole model is sufficient for these emitters, but it is powerless when l is a fraction for the emitters based on the cobweb structure, because l is considered an integer from the beginning of the model. What's more, to the best of our knowledge, there is no theoretical model for fractional topological charges l from integrated emitters so far what shows many applications such as rotating and manipulating microscopic particles [31]. Luckily, we can use Eq. (2) and Eq. (4) from the CWM to analyze them, which is a unique advantage of the model. Especially, we calculated the light for $l = 4.3$ by Eq. (2) and the results are shown in Fig. 3(a), (b). Moreover, we simulated the light for $l = 4.7$ by Eq. (4) with m from -40 to 40 in Fig. 3(c), (d). Those simulation results are consistent with the theoretical and experimental results in the previous report [32, Fig. 1(a), (b), (c)], which confirms the feasibility of the model.

Attributing to the completely diverse polarization distribution, the dipole model based on microring structure cannot be directly
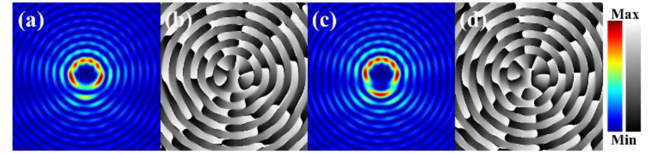

Fig. 3. Simulated light intensity and phase diagram of fractional topological charges in $N = 36$ devices and $\varphi = \pi/6$ $\vartheta = 0$. (a) Intensity and (b) Phase for $l = 4.3$ by Eq. (2). (c) Intensity and (d) Phase for $l = 4.7$ by Eq. (4) with m from -40 to 40.
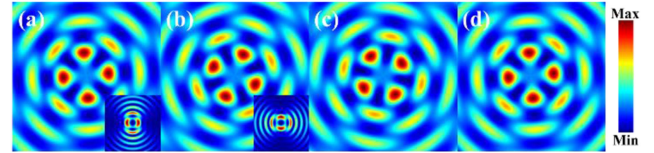

Fig. 4. Interference diagram of OAM beam with different initial polarization and spherical wave when $N = 32$, $l = 3$. (a) $\vartheta = 0$ and the inset shows E_x with any initial polarization. (b) $\vartheta = \pi/4$ and the inset shows E_y with any initial polarization. (c) $\vartheta = \pi/2$ (d) $\vartheta = 3\pi/4$.

applied to the cobweb structure. In addition, the dipole model cannot do anything to some devices with more general polarization state [12, Fig. 3(a)] since it does not consider the initial polarization of each emission point. Fortunately, our model considers these cases and introduces ϑ to reflect the effects of different initial polarization states on OAM beams. For example the initial polarization states is radially polarized for $\vartheta = 0$ and is azimuthally polarized for $\vartheta = \pi/2$. As we can see from Eq. (6) that ϑ only affects the phase for light field in far-field and has no effect on the polarization of the OAM beam. No matter from microring resonator structure or cobweb structure, the OAM beam in the far-field consists of $(l - pN) - 1$ order LHCP light and $(l - pN) + 1$ order RHCP light, which is a pioneering conclusion.

To manifest their dissimilarities of different initial polarization states, we use spherical waves to interfere with them. As shown in Fig. 4, the interference diagrams Fig. 4(a)–(d) are the interference results of spherical wave with OAM beams for $\vartheta = 0, \pi/4, \pi/2, 3\pi/4$ respectively. The results show that the four petals correspond to the topological charge of the vortex beam and when ϑ becomes larger, the petals rotate clockwise at a certain angle. Simultaneously, this rotation is related not only to the initial polarization distribution states, but also to the value of topological charge. Finally, we calculated the E_x [inset in Fig. 4(a)] and E_y [inset in Fig. 4(b)] of OAM beams with $\vartheta = 0, \pi/4, \pi/2, 3\pi/4$, which do not change with ϑ. This shows theoretically that the initial polarization state has no effect on the far-field polarization.

VI. CONCLUSION

In this paper, we have established, developed and verified a conical wave model, which regards the diffraction grating as a plane wave source. The wavefront of all plane waves forms a conical shape, and through strict calculation, we obtained that all wavelets interfere in the far field to form OAM beams, which

consists of $l - pN - 1$ order LHCP light and $l - pN + 1$ order RHCP light. The model has the following three advantages. First, the physical mechanism of the model is very distinct by approximating the light emitted from the grating with plane wave and directly calculating from the light field. Second, it can precisely calculate the distribution of light field when the topological charge is too large or fractional, which will provide a more comprehensive and accurate theoretical description for the application of OAM beams. Thirdly, by introducing ϑ to analyze the initial polarization state of the beam, the model can be applied to a variety of structures, such as micro ring resonator structure and cobweb structure as mentioned in the article.

Compared to the other previously theoretical models of integrated devices for vortex beam generation, our model have an accurate, intuitive and comprehensive result. The CWM is more concise and ocular than the coupled mode theory (see Eq. s17 in [1]), which only quantitatively illustrates the value of topological charges and the coupling process. What's more, at some points where the dipole model is break down, our model still works and can be calculated on fractional order beams. Although numerical methods such as FDTD or FEM (Finite Element Method) can give good results due to the rapid development of high performance computing, our model can give results in a shorter time, especially for devices with large size.

It is worth noting that this model is essentially different from the dipole model, because it replaces each emission grating with a plane wave source instead of dipole oscillator and start directly from the light field of plane wave instead of dipole moment. And it will be an arbitrary behavior to treat the conical wave model as a fairly straightforward extension of the dipole model since the former has been experimentally validated to treat the radiation grating as a planar wave source [17] and the latter not. As discussed in this paper, when l is small, the similarity between the two models is as high as 0.9919 for light intensity and 0.9893 for light phase, but when l gets larger, the similarity decreases gradually, which is the main advantage of this model. In addition, although FDTD or FEM is highly efficient and accurate, this does not mean that a new model is meaningless because time costs of using numerical methods will be extraordinary high for devices larger than 30 um.

In summary, the conical wave model have more generality results than above models or methods and when $\vartheta = 0$, $p = 0$ in Eq. (6), we can get the same result as the dipole model. What's more, it is also applicable to the theoretical analysis of generating OAM beams with fractional topological charges for integrated devices, which is a distinguishing feature from other analytical method or model. By using this model to analyze the far-field light field of different structures, we find that the different initial polarization states only affect the phase of the beam and they can get the same Ex and Ey results with different ϑ. This work can help people understand the generation mechanism of integrated OAM beam emitters more accurately and clearly. It will provide better theoretical support for OAM beam in engineering applications, such as optical micromanipulation, high-capacity optical communication, high-security encryption and so on.

REFERENCES

[1] X. Cai *et al.*, "Integrated compact optical vortex beam emitters," *Science*, vol. 338, no. 6105, pp. 363–366, Oct. 2012, doi: 10.1126/science.1226528.

[2] M. J. Strain *et al.*, "Fast electrical switching of orbital angular momentum modes using ultra-compact integrated vortex emitters," *Nat. Commun.*, vol. 5, Sep. 2014, Art. no. 4856, doi: 10.1038/ncomms5856.

[3] S. Li *et al.*, "Compact high-efficiency vortex beam emitter based on a silicon photonics micro-ring," *Opt. Lett.*, vol. 43, no. 6, pp. 1319–1322, Mar. 2018, doi: 10.1364/OL.43.001319.

[4] Z. Shao, J. Zhu, Y. Zhang, Y. Chen, and S. Yu, "On-chip switchable radially and azimuthally polarized vortex beam generation," *Opt. Lett.*, vol. 43, no. 6, pp. 1263–1266, Mar. 2018, doi: 10.1364/OL.43.001263.

[5] D. Zhang, X. Feng, and Y. Huang, "Encoding and decoding of orbital angular momentum for wireless optical interconnects on chip," *Opt. Exp.*, vol. 20, no. 24, pp. 26986–26995, Nov. 2012, doi: 10.1364/OE.20.026986.

[6] J. Sun, A. Yaacobi, M. Moresco, D. Coolbaugh, and M. R. Watts, "Integrated continuously tunable optical orbital angular momentum generator," in *Proc. CLEO Postdeadline Paper Digest*, 2015, Paper JTh5A-5.

[7] B. Guan *et al.*, "Free-space coherent optical communication with orbital angular, momentum multiplexing/demultiplexing using a hybrid 3D photonic integrated circuit," *Opt. Exp.*, vol. 22, no. 1, pp. 145–156, Jan. 2014, doi: 10.1364/OE.22.000145.

[8] Y. Wang *et al.*, "Integrated photonic emitter with a wide switching range of orbital angular momentum modes," *Sci. Rep.*, vol. 6, Mar. 2016, Art. no. 22512, doi: 10.1038/srep22512.

[9] Y. X. Chen, Z. J. Lin, S. Belanger-de Villers, L. A. Rusch, and W. Shi, "WDM-Compatible polarization-diverse OAM generator and multiplexer in silicon photonics," *IEEE J. Sel. Topics Quantum Electron.*, vol. 26, no. 2, Mar./Apr. 2020, Art. no. 6100107, doi: 10.1109/jstqe.2019.2941488.

[10] K. P. Huy, A. Morand, D. Amans, and P. Benech, "Analytical study of the whispering-gallery mode in two-dimensional microgear cavity using coupled-mode theory," *J. Opt. Soc. Amer. B-Opt. Phys.*, vol. 22, no. 8, pp. 1793–1803, Aug. 2005, doi: 10.1364/JOSAB.22.001793.

[11] N. Zhang, J. Zhu, X. Cai, and S. Yu, "Coupled mode analysis of angular grating-based optical vortex beam emitters," in *Proc. Asia Commun. Photon. Conf.,* 2014, Paper AW3B-1.

[12] Y. F. Yu *et al.*, "Pure angular momentum generator using a ring resonator," *Opt. Exp.*, vol. 18, no. 21, pp. 21651–21662, Oct. 2010, doi: 10.1364/OE.18.021651.

[13] M. Fujita and T. Baba, "Proposal and finite-difference time-domain simulation of whispering gallery mode microgear cavity," *IEEE J. Quantum Electron.*, vol. 37, no. 10, pp. 1253–1258, Oct. 2001, doi: 10.1109/3.952536.

[14] R. Li, X. Feng, D. K. Zhang, K. Y. Cui, F. Liu, and Y. D. Huang, "Radially polarized orbital angular momentum beam emitter based on shallow-ridge silicon microring cavity," *IEEE Photon. J.*, vol. 6, no. 3, Jun. 2014, Art. no. 2200710, doi: 10.1109/jphot.2014.2321757.

[15] J. Zhu, X. Cai, Y. Chen, and S. Yu, "Theoretical model for angular grating-based integrated optical vortex beam emitters," *Opt. Lett.*, vol. 38, no. 8, pp. 1343–1345, Apr. 2013, doi: 10.1364/OL.38.001343.

[16] C. Z. Sun *et al.*, "Analysis of OAM mode purity of integrated optical vortex beam emitters," *IEEE Photon. J.*, vol. 9, no. 1, Feb. 2017, Art. no. 6600107, doi: 10.1109/jphot.2017.2652722.

[17] J. Du and J. Wang, "Chip-scale optical vortex lattice generator on a silicon platform," *Opt. Lett.*, vol. 42, no. 23, pp. 5054–5057, Dec. 2017, doi: 10.1364/OL.42.005054.

[18] I. A. Litvin, M. G. McLaren, and A. Forbes, "A conical wave approach to calculating Bessel–Gauss beam reconstruction after complex obstacles," *Opt. Commun.*, vol. 282, no. 6, pp. 1078–1082, Mar. 2009, doi: 10.1016/j.optcom.2008.11.079.

[19] D. McGloin and K. Dholakia, "Bessel beams: Diffraction in a new light," *Contemporary Phys.*, vol. 46, no. 1, pp. 15–28, Jan./Feb. 2005, doi: 10.1080/0010751042000275259.

[20] Y. Wang, P. Zhao, X. Feng, K. Cui, and Y. Huang, "Integrated emitters for optical vortices with a 'cobweb' structure," in *Proc. Opto-Electron. Commun. Conf.,* 2015, pp. 1–3.

[21] C. R. Doerr and L. L. Buhl, "Circular grating coupler for creating focused azimuthally and radially polarized beams," *Opt. Lett.*, vol. 36, no. 7, pp. 1209–1211, Apr. 2011, doi: 10.1364/OL.36.001209.

[22] T. Su *et al.*, "Demonstration of free space coherent optical communication using integrated silicon photonic orbital angular momentum devices," *Opt. Exp.*, vol. 20, no. 9, pp. 9396–9402, Apr. 2012, doi: 10.1364/OE.20.009396.

[23] N. K. Fontaine, C. R. Doerr, and L. L. Buhl, "Efficient multiplexing and demultiplexing of free-space orbital angular momentum using photonic integrated circuits," in *Proc. Opt. Fiber Commun. Conf.,* 2012, pp. 1–3.

[24] T. Irimatsugawa, Y. Shimizu, S. Okubo, and H. Inaba, "Cosine similarity for quantitatively evaluating the degree of change in an optical frequency comb spectra," *Opt. Exp.*, vol. 29, no. 22, pp. 35613–35622, Oct. 2021, doi: 10.1364/oe.435679.

[25] D. Zhuang *et al.*, "Omnidirectional beam steering using aperiodic optical phased array with high error margin," *Opt. Exp.*, vol. 26, no. 15, pp. 19154–19170, Jul. 2018, doi: 10.1364/OE.26.019154.

[26] C. Zhao and Y. Cai, "Trapping two types of particles using a focused partially coherent elegant Laguerre–Gaussian beam," *Opt. Lett.*, vol. 36, no. 12, pp. 2251–2253, Jun. 2011, doi: 10.1364/OL.36.002251.

[27] Z. Xu, X. Li, X. Liu, S. A. Ponomarenko, Y. Cai, and C. Liang, "Vortex preserving statistical optical beams," *Opt. Exp.*, vol. 28, no. 6, pp. 8475–8483, Mar. 2020, doi: 10.1364/OE.387181.

[28] D. G. Grier, "A revolution in optical manipulation," *Nature*, vol. 424, no. 6950, pp. 810–816, Aug. 2003, doi: 10.1038/nature01935.

[29] J. Wang *et al.*, "Terabit free-space data transmission employing orbital angular momentum multiplexing," *Nature Photon.*, vol. 6, no. 7, pp. 488–496, 2012, doi: 10.1038/nphoton.2012.138.

[30] X. Fang, H. Ren, and M. Gu, "Orbital angular momentum holography for high-security encryption," *Nat. Photon.*, vol. 14, no. 2, pp. 102–108, 2019, doi: 10.1038/s41566-019-0560-x.

[31] S. Tao, X. C. Yuan, J. Lin, X. Peng, and H. Niu, "Fractional optical vortex beam induced rotation of particles," *Opt. Exp.*, vol. 13, no. 20, pp. 7726–7731, Oct. 2005, doi: 10.1364/OPEX.13.007726.

[32] J. C. Gutiérrez-Vega and C. López-Mariscal, "Nondiffracting vortex beams with continuous orbital angular momentum order dependence," *J. Opt. A: Pure Appl. Opt.*, vol. 10, no. 1, pp. 015009–015016, 2008, doi: 10.1088/1464-4258/10/01/015009.